Acta Pharmaceutica Sinica B 2024;14(2):881−892

Chinese Pharmaceutical Association
Institute of Materia Medica, Chinese Academy of Medical Sciences

Acta Pharmaceutica Sinica B

www.elsevier.com/locate/apsb
www.sciencedirect.com

ORIGINAL ARTICLE

Disulfide bridge-targeted metabolome mining unravels an antiparkinsonian peptide

Zhiwu Tong[a,†], Xiahong Xie[b,†], Huiming Ge[a], Ruihua Jiao[a], Tingting Wang[a], Xincun Wang[c], Wenying Zhuang[c], Gang Hu[b,*], Renxiang Tan[a,b,*]

[a]*State Key Laboratory of Pharmaceutical Biotechnology, Institute of Functional Biomolecules, School of Life Sciences, Nanjing University, Nanjing 210023, China*
[b]*State Key Laboratory Cultivation Base for TCM Quality and Efficacy, Nanjing University of Chinese Medicine, Nanjing 210023, China*
[c]*Institute of Microbiology, Chinese Academy of Sciences, Beijing 100101, China*

Received 14 July 2023; received in revised form 6 September 2023; accepted 13 September 2023

KEY WORDS

Fungal RiPPs;
Biosynthesis;
Macrocyclic peptide;
Acalitide;
Antiparkinsonian

Abstract Peptides are a particular molecule class with inherent attributes of some small-molecule drugs and macromolecular biologics, thereby inspiring continuous searches for peptides with therapeutic and/or agrochemical potentials. However, the success rate is decreasing, presumably because many interesting but less-abundant peptides are so scarce or labile that they are likely 'overlooked' during the characterization effort. Here, we present the biochemical characterization and druggability improvement of an unprecedented minor fungal RiPP (ribosomally synthesized and post-translationally modified peptide), named acalitide, by taking the relevant advantages of metabolomics approach and disulfide-bridged substructure which is more frequently imprinted in the marketed peptide drug molecules. Acalitide is biosynthetically unique in the macrotricyclization *via* two disulfide bridges and a protease (AcaB)-catalyzed lactamization of AcaA, an unprecedented precursor peptide. Such a biosynthetic logic was successfully re-edited for its sample supply renewal to facilitate the identification of the *in vitro* and *in vivo* antiparkinsonian efficacy of acalitide which was further confirmed safe and rendered brain-targetable by the liposome encapsulation strategy. Taken together, the work updates the mining strategy and biosynthetic complexity of RiPPs to unravel an antiparkinsonian drug candidate valuable for combating Parkinson's disease that is globally prevailing in an alarming manner.

*Corresponding authors.
E-mail addresses: ghu@njmu.edu.cn (Gang Hu), rxtan@nju.edu.cn (Renxiang Tan).
[†]These authors made equal contributions to this work.
Peer review under the responsibility of Chinese Pharmaceutical Association and Institute of Materia Medica, Chinese Academy of Medical Sciences.

https://doi.org/10.1016/j.apsb.2023.09.006

1. Introduction

Peptides represent a distinct compound class that is documented to possess some attributes of both small-molecule drugs and macromolecular biologics such as peptide-based enzymes, hormones, and physiological mediators[1,2]. This observation, along with the one-century application of insulin (the first peptide-based drug), keeps inspiring the global search for more peptide therapeutics urgently required for combating currently unsolved health issues such as most of the aging-related diseases[1,3]. However, peptides are more frequently proven to be poorly druggable because of some inherent shortcomings including but not limited to the unstability (readily cleaved by proteolytic enzymes), poor oral bioavailability and fast clearance (rapidly metabolized by enzymes), and membrane impermeability resulting largely from the ionic and hydrophilic amino acid (AA) residues[1]. Encouragingly, the cyclization of peptide chains can more or less improve the structural and pharmacokinetic properties for absorption, distribution, and cell membrane permeability, thereby explaining why two-thirds of the US Food and Drug Administration (FDA)- and European Medicines Agency (EMA)-approved peptide drugs are in the cyclic form[2]. More impressively, eight out of the 18 cyclic peptide drugs approved from 2001 through 2021 possess disulfide-bridged motifs (Supporting Information Fig. S1)[2]. In some cases as reviewed[4], cyclic peptides with disulfide bridges seem more druggable than the disulfide-free counterparts, in view of the disulfide bridge-conferred resistance to chemical and enzymatic degradations. Furthermore, disulfide bonds can decrease the conformational flexibility of polypeptides, which is involved in exerting their biological functions[4]. The question that follows is where and how to find the undescribed disulfide-bridged peptide with medical significance. This work identifies a minor thus previously overlooked representative by locking on the general characteristics of such peptides during the preliminary assay (*vide infra*).

The rapid advancement of gene sequencing and genome mining technologies has accelerated the characterization of ribosomally synthesized and post-translationally modified peptides (RiPPs) from plants and bacteria[5–7], but rarely from fungi. Since the first fungal RiPP was reported in 2007[8], only a handful of RiPPs have been discovered[9]. Nonetheless, fungal RiPPs seem biosynthetically diverse as showcased by peptides belonging to the dikaritin, borosin and cycloamanide families (Fig. 1 and Supporting Information Table S1)[9]. The dikaritin cyclopeptides, such as asperipin-2a, are macrocyclized from kexin protease-processed precursor peptides through the DUF3328 protein-catalyzed ether bond formation[10–14]. The precursor peptides of borosin cyclopeptides are usually fused to *N*-methyltransferase catalyzing the *N*-methylation steps, while the head-to-tail macrocyclization is catalyzed by the prolyl oligopeptidase (OphP) as exemplified by the omphalotin H construction (Fig. 1)[15–18]. The cycloamanide-typed RiPPs (*e,g.*, cycloamanide B) are biosynthetically characterized by the prolyl oligopeptidase B (POPB)-catalyzed truncation and macrocyclization of precursor peptides with the conserved (MSDIN) N-terminal motifs[19,20]. However, to our surprise, few of the fungal RiPPs characterized so far are disulfide-bridged. The observation motivated us to search for architecturally unprecedented fungal RiPPs with disulfide bridge(s) and potent bioactivity. Here, we report the structure, biosynthetic pathway, sample supply renewal, and antiparkinsonian efficacy of acalitide, a novel fungal RiPP with two disulfide bridges, to provide an unprecedented starting molecule valuable for the search of new drugs counteracting Parkinson's disease.

2. Results and discussion

2.1. Discovery of acalitide

In theory, the metabolomics approach can provide the global metabolite profiles for a given biological system (cell, tissue, or organism), but in practice, the methodology is more or less 'inactivated' by the lability or poor abundance of some metabolites such as unstable or less-abundant peptides, which are either decomposed during the analysis or exist below/around the instrument detection limit. It is even more challenging to characterize the undescribed fungal RiPPs, many of which could be too scarce to be detected directly from the fungal culture by liquid chromatography-high resolution mass spectrometry (LC−HRMS). We envisioned that the removal of dominant substances from the fungal culture-derived extract might allow for the detection of less-abundant chemicals including RiPP(s). On the other hand, there has been no established methodology specific for multi-sulphur peptides. However, a literature search allowed us to perceive that multi-sulphur peptides display polysulfurated molecular formulas and intense molecular ion peaks because their MS fragmentation is substantially reduced or prohibited by the disulfide bridges. With the rationalizations in mind, a collection of mother liquors left over after our isolation of acatulides[21], acautalides[22], acaulins[23], and acaulide[24] from the *Acaulium album* culture was re-analysed by LC−HRMS with an intention of hitting the multi-sulphur peptide(s). Such an effort allowed us to come across a peptide-like compound with its molecular formula evidenced, and confirmed after its purification, to be $C_{127}H_{193}N_{31}O_{32}S_4$ from its doubly protonated molecular ion ($[M+2H]^{2+}$) at *m/z* 1397.1811 (the half of $C_{127}H_{195}N_{31}O_{32}S_4$ requires 1397.1806) (Fig. 2A). This MS spectral feature was unprecedented suggesting that it was most likely an undescribed peptide chemical entity. We therefore named the peptide acalitide for simplicity. The structural complexity of acalitide displayed highly-overlapped signals in its ^{1}H and ^{13}C nuclear magnetic resonance (NMR) spectra (Supporting Information Figs. S2−S9), in which only the resonance arising from a few of AA residues could be assigned with an aid of two-dimensional (2D) NMR experiments (Supporting Information Table S2). Fortunately, our efforts for the acalitide structure was rendered successful by obtaining its crystallographic structure. The low-temperature single-crystal X-ray diffraction analysis of the crystal of acalitide (CCDC deposition number 1985321) with Cu Kα radiation (configuration with a Flack parameter of 0.031(9)), underpinning that it was a macrocyclic peptide composed of thirty AA residues.

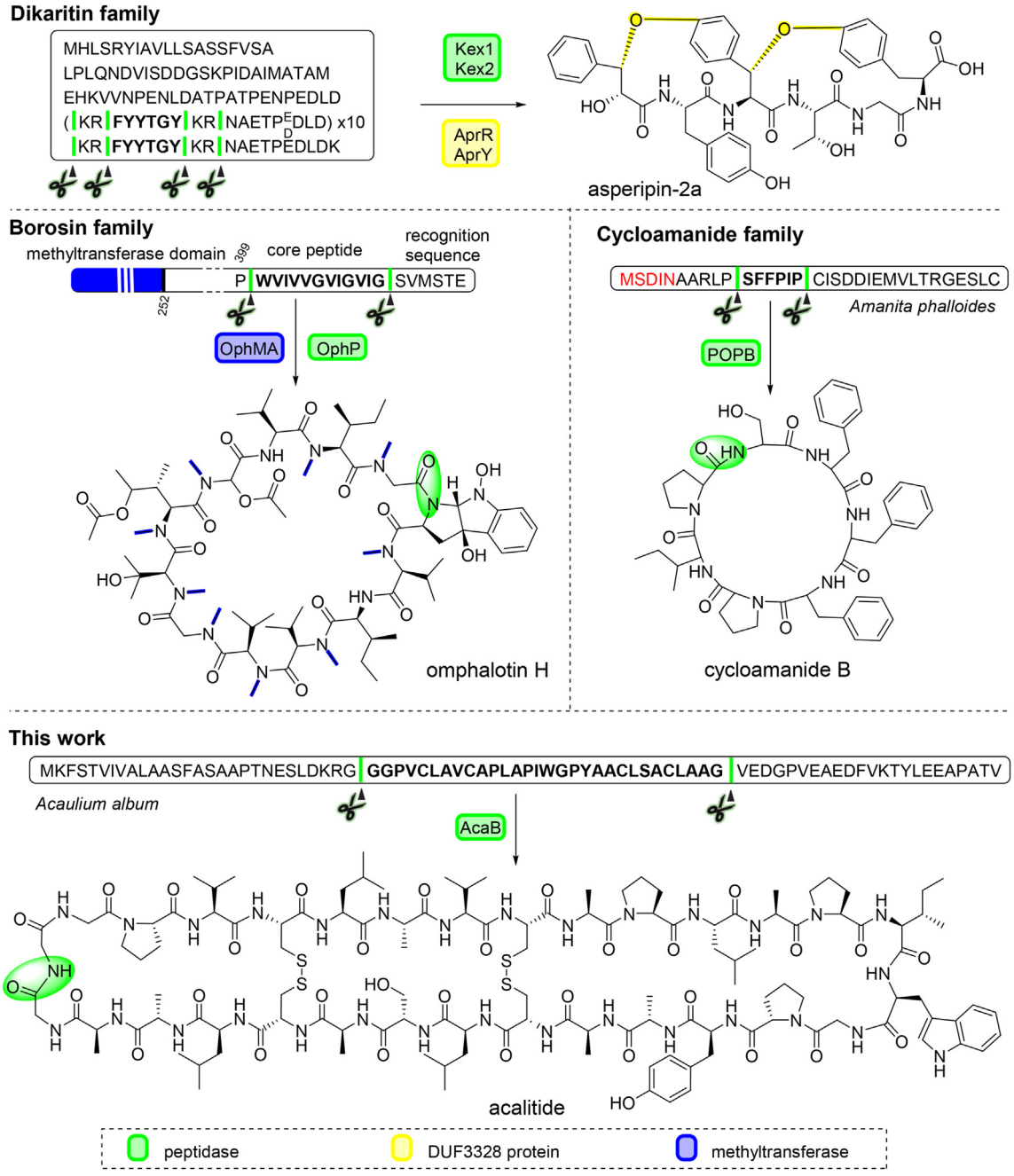

Figure 1 Biosynthetic characteristics of representative fungal RiPPs families. Proteins and relevant structural motifs/bonds they are responsible for are shaded with matching color. In precursor peptide sequences, the core peptide is highlighted in bold and cut-sites are indicated as vertical lines. The red font in the cycloamanide family indicates the N-terminal conserved amino acid sequence.

The X-ray crystallographic interpretation established the structure of acalitide as cyclo-(Cys^{22}-Leu^{23}-Ser^{24}-Ala^{25}-Cys^{26}-Leu^{27}-Ala^{28}-Ala^{29}-Gly^{30}-Gly^{1}-Gly^{2}-Pro^{3}-Val^{4}-Cys^{5}-Leu^{6}-Ala^{7}-Val^{8}-Cys^{9}-Ala^{10}-Pro^{11}-Leu^{12}-Ala^{13}-Pro^{14}-Ile^{15}-Trp^{16}-Gly^{17}-Pro^{18}-Tyr^{19}-Ala^{20}-Ala^{21}) and the two disulfide bonds form from four cysteine residues (Cys^{5}, Cys^{9}, Cys^{22} and Cys^{26}) (Fig. 2B and Supporting Information Fig. S11). Moreover, the X-ray crystallography highlighted that all AA residues of acalitide shared the L-configuration (Fig. 2B). To our knowledge, acalitide is the first RiPP which is unique in its macrotricyclization *via* two disulfide bridges and an amide bond, and thus distinct from the counterparts characterized so far[7,9].

2.2. *The biosynthetic pathway of acalitide*

The unique structure of acalitide tempted us to address its biosynthetic pathway. Therefore, the *A. album* genome was sequenced and searched for the biosynthetic genes that governs the acalitide assembly. The structural feature of acalitide suggested that it could be either ribosomally-synthesized and post-translationally modified, or synthesized by non-ribosomal peptide synthetase (NRPS). Accordingly, the fungal genome was analyzed through AUGUSTUS, 2ndFind, and antiSMASH softwares, indicating that it has four NRPS-encoding genes; but

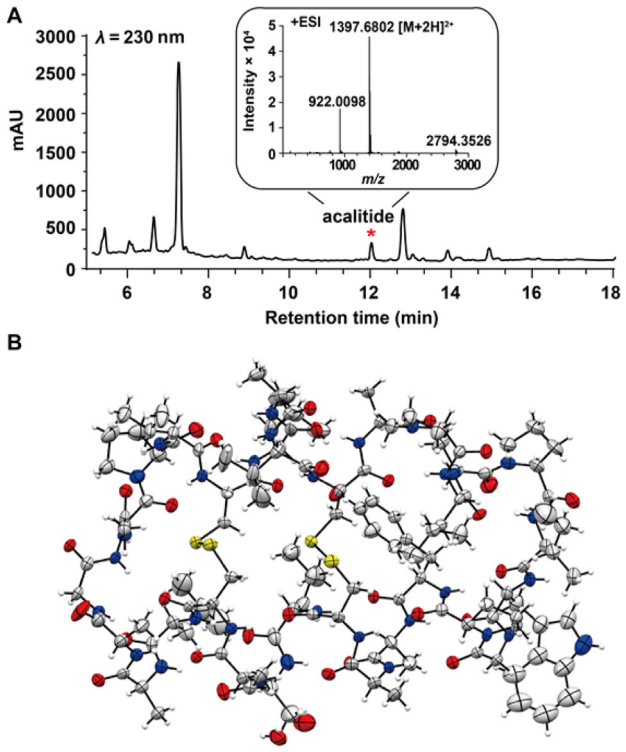

Figure 2 Discovery of acalitide. (A) the LC−HRMS detection of acalitide as a low-abundance peptide from *Acaulium album*. Mass recalibration was accomplished by referring to the $[M+H]^+$ peak at *m/z* 922.0098 of hexakis-(2,2,3,3,-tetrafluoropropoxy)-phosphazine. (B) Crystal structure of acalitide with co-crystalized solvent molecules omitted for clarity. ESI, electron spray ionization.

none of them was predicted to be responsible for the acalitide biosynthesis. Next, we sliced the 30-AA cyclopeptide at 29 positions to obtain a total of 30 sequence-overlapping 'linear peptide domains'. With that, we searched the translated *A. album* genome for matched peptide domain(s). As a result, two sequences (Gly^{30}-Gly^{1}-Gly^{2}-Pro^{3}-Val^{4}-Cys^{5}-Leu^{6}-Ala^{7}-Val^{8}-Cys^{9}-Ala^{10}-Pro^{11}-Leu^{12}-Ala^{13}-Pro^{14}-Ile^{15}-Trp^{16}-Gly^{17}-Pro^{18}-Tyr^{19}-Ala^{20}-Ala^{21}-Cys^{22}-Leu^{23}-Ser^{24}-Ala^{25}-Cys^{26}-Leu^{27}-Ala^{28}-Ala^{29}, and Gly^{1}-Gly^{2}-Pro^{3}-Val^{4}-Cys^{5}-Leu^{6}-Ala^{7}-Val^{8}-Cys^{9}-Ala^{10}-Pro^{11}-Leu^{12}-Ala^{13}-Pro^{14}-Ile^{15}-Trp^{16}-Gly^{17}-Pro^{18}-Tyr^{19}-Ala^{20}-Ala^{21}-Cys^{22}-Leu^{23}-Ser^{24}-Ala^{25}-Cys^{26}-Leu^{27}-Ala^{28}-Ala^{29}-Gly^{30}) were found to match the middle of an open-reading frame encoding a peptide consisting of 81 AA residues. The observation confirmed acalitide as a RiPP and highlighted its precursor peptide-encoding gene which we have named *acaA*. As suggested by its structure, the acalitide biosynthesis requires a peptidase to truncate AcaA. We therefore re-analysed the fungal genome to recognize a peptidase-encoding gene named *acaB* (GenBank accession number OP150447) (Fig. 3A). The *acaB* gene function was confirmed by cloning the *acaAB* genes in pUSA and pTAex3 plasmids, respectively, both being transferred to *Aspergillus oryzae* (AO) NSAR1 (Supporting Information Fig. S12). Gratifyingly, acalitide appeared in the culture of the AO-*acaAB* transformant (Fig. 3B), underscoring that the acalitide formation from precursor peptide (AcaA) required AcaB, a peptidase catalyzing the macrocyclization by cleaving off the N- (leader) and C-terminal (follower) peptide domains of AcaA. Unfortunately, we failed in expressing AcaA and AcaB in *Escherichia coli* BL21 (DE3), presumably because of the evolutionary distance between fungi and bacteria (Supporting Information Fig. S13).

The assembly of cyclotides, which are cyclic peptides typically with three disulfide bridges, is preconditioned by the 'faster formation' of disulfide bonds that confer the precursor peptide resistant to enzymatic and acidic degradation ahead of the head-to-tail cyclization[25]. Such intramolecular disulfide bonds are most likely generated under the catalysis of the protein disulfide isomerases (PDIs), which are ubiquitous in the endoplasmic reticulum (ER) and essential for the viability of eukaryotic microorganisms[26,27]. However, the two AcaA-matched sequences (*vide supra*) allowed two cyclization options to form acalitide, namely through the amide bond formation of either $AcaA^{G28}$ with $AcaA^{A57}$ or $AcaA^{G29}$ with $AcaA^{G58}$ (Fig. 3A). To address the ambiguity, we generated two single-point muted (AO-*acaA*^{G28A}*B* and AO-*acaA*^{G58A}*B*) transformants (Supporting Information Table S4). As shown in Fig. 3C, acalitide was detected in the culture of the AO-*acaA*^{G28A}*B* mutant rather than the AO-*acaA*^{G58A}*B* strain. The observation clarified that AcaA cyclized into acalitide *via* the amide bond between the G29 and G58 residues of AcaA under the AcaB catalysis. More noteworthily, AcaA was evidenced to be an unprecedented precursor peptide with its N-terminal AA sequence entirely different from the described counterparts (Fig. 1 and Table S1)[9]. Taken together, the trimacrotricyclization of acalitide is realized through an amide bond and two disulfide bridges, and this is distinct from the construction pattern of reported RiPPs such as those formulated in Fig. 1.

2.3. *Renewed sample supply for acalitide*

Many peptides are biologically potent and some are commercialized products[7]. But acalitide was characterized as a minor peptide from the mother liquor left over after purifying abundant metabolites from the fungal culture (*vide supra*). We consequently sought to establish an alternative access to acalitide for a sufficient amount of sample so that it could be bio-evaluated in as diverse models as possible. Because the reproduction rate of fungi is generally slower than bacteria, *E. coli* was tested as a vector for a more efficient generation of acalitide. However, likely owing to the difference in the intracellular structure between fungi and bacteria, acalitide failed to form in the bacterium (Fig. 4, traces ii). Nonetheless, the aforementioned expression of acalitide in AO encouraged us to optimize the cultivation of the AO-*acaAB* transformant to make acalitide more abundant than in the *A. album* culture (Fig. 4, traces iii and iv). In hoping so, another copy of *acaAB* genes was integrated into the AO-*acaAB* strain to give the two-copy (AO-2 × *acaAB*) transformant. Gratifyingly, the acalitide abundance in the 3-day cultivation of the AO-2 × *acaAB* strain were 3 and 30 times higher than in the AO-*acaAB* transformant and native fungal producer (Fig. 4, traces iii and v), respectively. Using the two-copy transformant, we were able to produce more acalitide sample for its bioactivity bioassay in diverse models (*vide infra*).

2.4. *Identification of acalitide as an antiparkinsonian drug candidate*

2.4.1. *In vitro and in vivo neuroprotectivity of acalitide*

With the sample supply guaranteed, acalitide was bio-assessed in a 'compound-centric' manner which is characterized by evaluating a single sample in a possibly wide range of bioassay models till its biological property of interest was found. After tested against diverse targets (Supporting Information Table S5), acalitide was shown to improve the viability of the MPP^+ (1-methyl-4-phenylpyridinium)-injured human dopaminergic SH-SY5Y cells in a dose-dependent

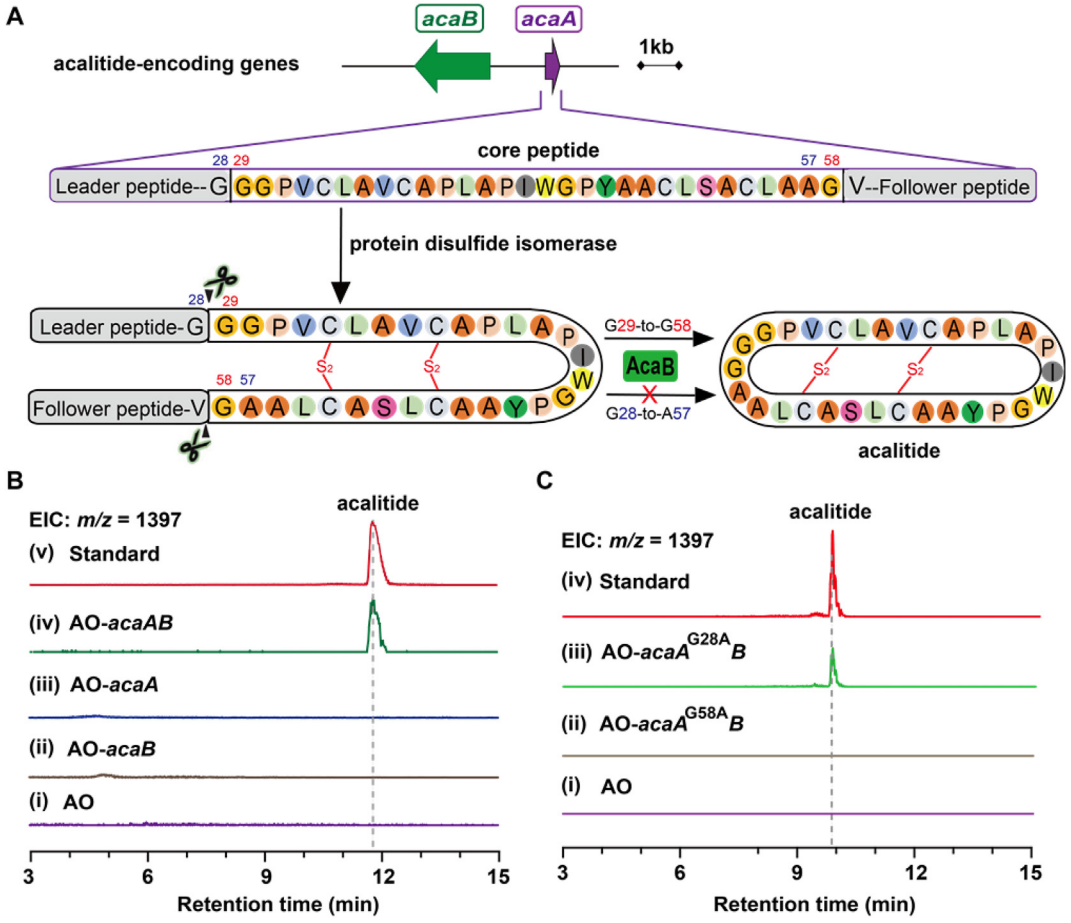

Figure 3 Biosynthesis and heterologous expression of acalitide. (A) Acalitide assembly in *A. album* under the governance of the *acaA* and *acaB* genes encoding precursor peptide and peptidase, respectively. The disulfide bridge formation is likely catalyzed by protein disulfide isomerase ubiquitous in the eukaryotic endoplasmic reticulum[27]. (B) Reconstitution of the acalitide biosynthesis in *Aspergillus oryzae* (AO). (i) the AO wild-type strain; (ii−iv) AO-*acaB*, AO-*acaA* and AO-*acaAB* transformants, respectively; (v) standard of acalitide. (C) Site-directed mutagenesis of AcaA. (i) the AO wild-type strain; (ii and iii) AO-*acaA*^{G58A}*B* and AO-*acaA*^{G28A}*B* mutants, respectively; (iv) Standard of acalitide. The extracted ion chromatograms (EICs) were extracted at *m/z* 1397 $[M+2H]^{2+}$ for acalitide.

manner in a dose range of 10 nmol/L to 1 μmol/L (Supporting Information Fig. S14A and S14B). Furthermore, acalitide effectively mitigated the MPP^+-imposed damage to mouse neuronal synapses (Fig. 5A and Fig. S14C). The neuroprotective effect of acalitide was reinforced by our cell apoptosis assay using Annexin V (AV)/propidium iodide (PI) and Hoechst 33,258 stainings (Fig. 5B−D). Next, the *in vivo* neuroprotectivity of acalitide was assessed using *Caenorhabditis elegans* BZ555 [dat-1p::GFP], an *in vivo* (nematode) model of Parkinson's disease (PD)[28]. Ascertaining that acalitide increased the survival rate of the MPP^+-treated nematodes (Supporting Information Fig. S15A), the swimming induced paralysis (SWIP) assay was performed to assess the dopamine signaling. Acalitide could counteract the inappropriate motor behavior after the MPP^+ challenge (Fig. S15B). Furthermore, acalitide reversed the MPP^+ damage to dopaminergic neurons as indicated by the green fluorescent protein (GFP) fluorescence that was as bright and massive as was the treatment with amantadine co-assayed a positive control in the study (Fig. 5E). In particular, acalitide was shown to be more protective than amantadine in counteracting the MPP^+ injury (Fig. 5F). This set of experimentations underpinned that acalitide surpassed amantadine in preventing the MPP^+-caused damage to the nematode dopaminergic neurons.

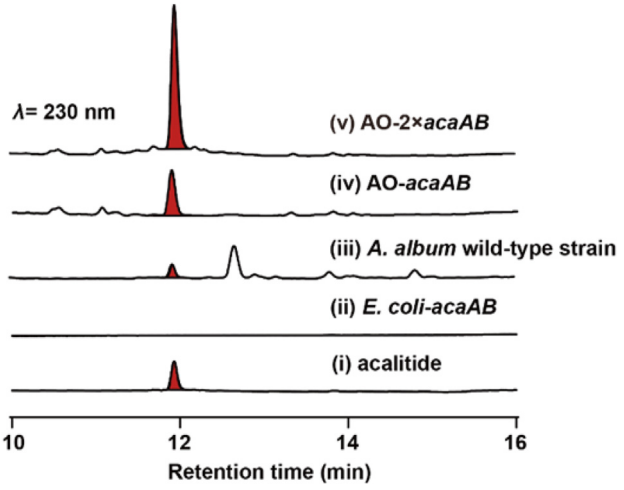

Figure 4 The sample supply renewal for acalitide. (i) Standard of acalitide; (ii) *E. coli*-acaAB transformant that did not produce acalitide; (iii) Acalitide appeared at around 0.18 mg/L in the *A. album* culture; (iv and v) AO-acaAB and AO-2 × acaAB transformants produced acalitide at titers of 2.0 and 5.7 mg/L, respectively. AO, *Aspergillus oryzae* NSAR1.

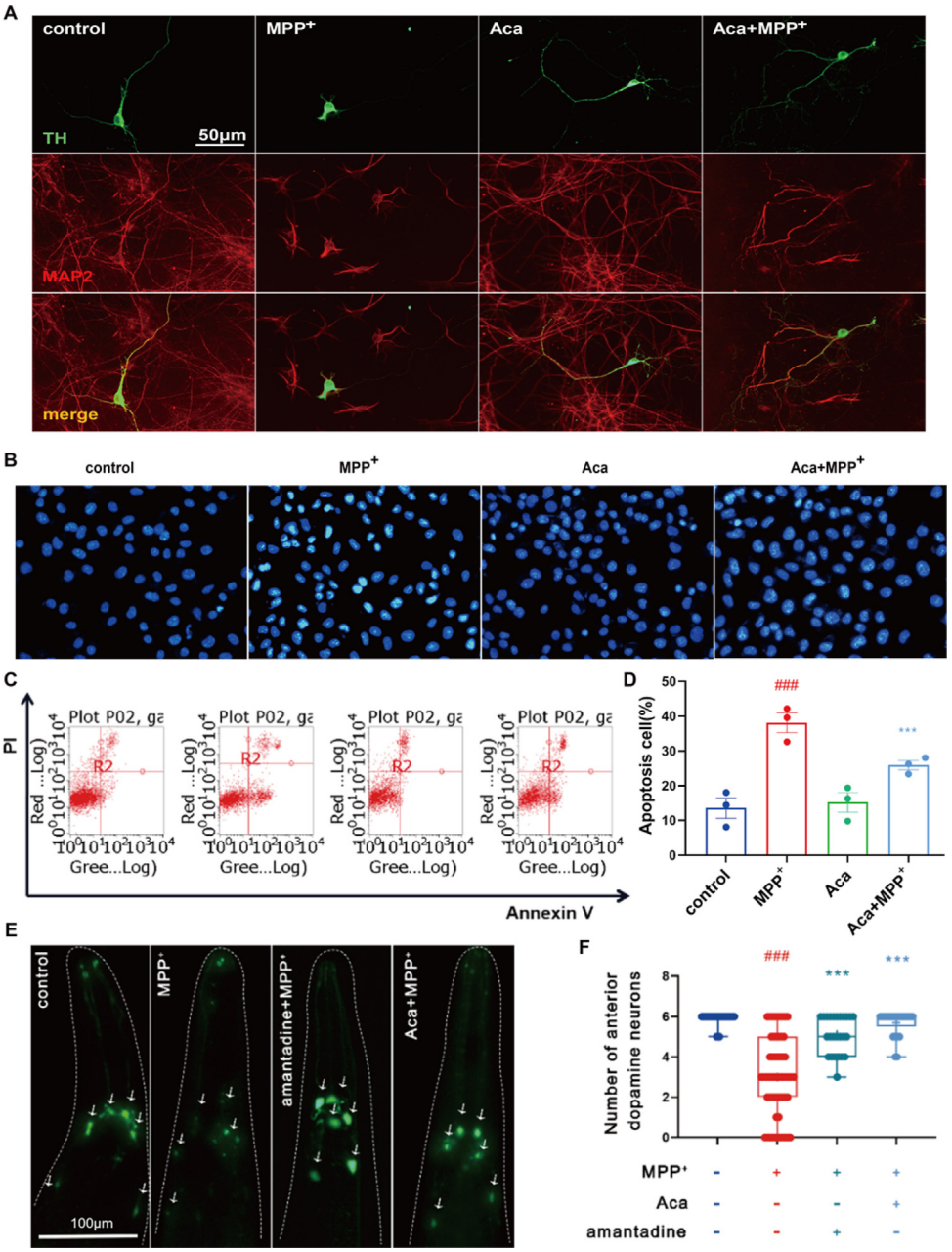

Figure 5 *In vitro* and *in vivo* neuroprotectivity of acalitide (Aca). (A) Acalitide protected the MPP^+-induced damage to neuronal synapses as corroborated by fluorescent images of mouse midbrain primary neurons cultured for 7 days with tyrosine hydroxylase (TH, green) and microtubule-associated protein 2 (MAP2, red) stainings. (B) Acalitide reverses SH-SY5Y cell apoptosis evaluated by Hoechst 33,258 staining. (C) The protective effect of acalitide on MPP^+ insulted SH-SY5Y cells were confirmed by annexin V (AV)-propidium iodide (PI) staining and flow cytometry analysis. (D) Acalitide reduces the MPP^+-induced apoptosis of SH-SY5Y cells as indicated by staining with Annexin V and PI (propidium iodide) using flow cytometry. (E−F) Acalitide reversed the MPP^+-damage to dopaminergic neurons in the nematode head as demonstrated by immunofluorescence images (E) and quantity statistics (F) on the anterior dopamine neurons. Amantadine, a clinical drug used as a positive control. The scale bar is 100 μmol/L. The data are the mean ± SEM. $^{***}P < 0.001$ *vs* MPP $^+$ group, $^{\#\#\#}P < 0.001$ *vs* control group are analyzed with One-way-ANOVA, $n \geq 30$ for each group. MPP^+, 1-methyl-4-phenylpyridinium.

2.4.2. Preparation of nanoliposomes and evaluation of acalitide neuroprotective activity in mice model

To address whether acalitide is neuroprotective in mammals, we generated the subacute PD model by treating mice with 1-methyl-4-phenyl-1,2,3,6-tetrahydropyridine (MPTP) that selectively injures nigrostriatal dopaminergic neurons[29]. To our surprise, acalitide displayed negligible efficacy in the MPTP-challenged mice (Fig. 7C). We envisioned that acalitide is hydrophobic and likely difficult to enrich in mouse brain *via* its penetration across the blood−brain barrier (BBB). Inspired by the BBB permeability of paeoniflorin-loaded nanosheets (mean diameter: 203 nm)[30], we encapsulated acalitide in the long-circulating liposome (LCL) prepared from 1,2-distearoyl-*sn*-glycero-3-phosphoethanolamine-*N*-[methoxy(polyethyleneglycol)-2000](DSPE-PEG2000) and its glycolate (DSPE-PEG2000-COOH), since such LCLs were validated to be effective carrier for drug delivery to brain with

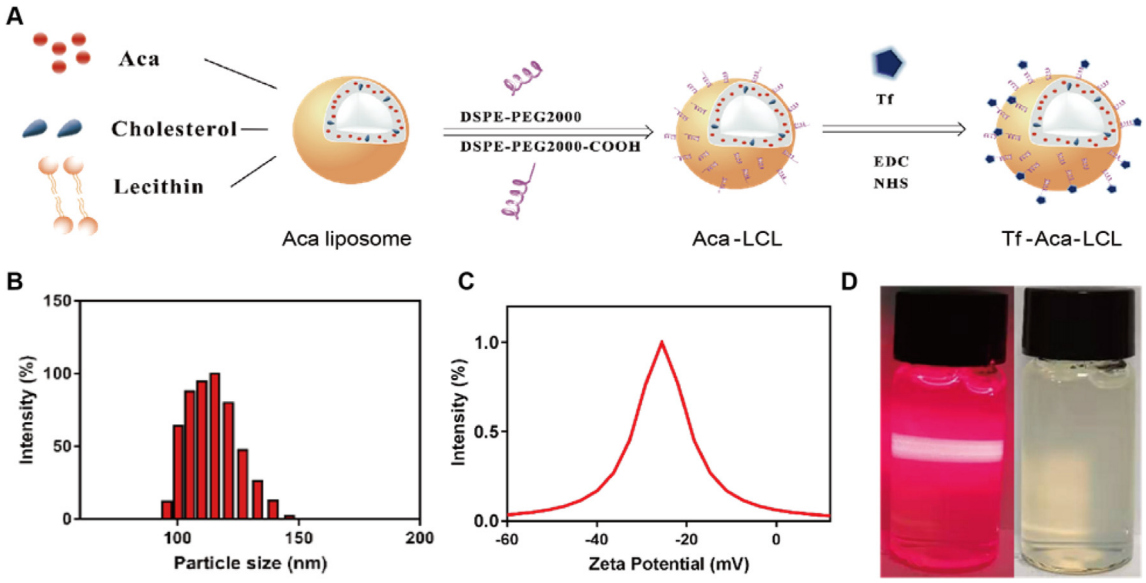

Figure 6 Characterization of Tf-Aca-LCL. (A) Schematic diagram of the preparation of Tf-Aca-LCL. (B) Particle size distribution of Tf-Aca-LCL, the size is 115.53 ± 4.44 nm (n = 3). (C) Zeta Potential rang is −25.5 ± 2.94 mV (n = 3). (D) Appearance of Tf-Aca-LCL. Aca, acalitide. Tf-Aca-LCL, defined in the text.

prolonged *in vivo* clearance over drugs alone[31,32]. Technically, the acalitide-embedded LCL liposome (Aca-LCL) was synthesized in a size-controlled manner from an optimized mixture of DSPE-PEG2000 and DSPE-PEG2000-COOH (Fig. 6A), in viewing that nanoparticles in 100−300 nm size are BBB-penetrable[33,34]. To further enhance its brain targeting property, Aca-LCL was installed with surface-bound transferrin (Tf) to form Tf-Aca-LCL, which was shown to have an improved affinity to the transferrin receptor (TfR) on the surface of nigral dopaminergic neurons (Fig. 6B−D)[35]. To address whether Tf-Aca-LCL was BBB-penetrable, a fluorescent agent called IR780 {2-[2-[2-chloro-3-[(1,3-dihydro-3,3-dimethyl-1-propyl-2*H*-indol-2-ylidene)ethylidene]-1-cyclohexen-1-yl]ethenyl]-3,3-dimethyl-1-propylindolium iodide} was encapsulated along with acalitide to afford Tf-Aca-LCL-IR780 (Fig. 7A). As desired, the *in vivo* fluorescence imaging (Fig. 7B) showed that Tf-Aca-LCL-IR780 reached the mouse brain and culminated 6 h after being administered *via* tail vein injection. As shown in Fig. 7C and D, when delivered as long-circulating liposome (Tf-Aca-LCL), acalitide was at least as efficacious as amantadine in rescuing the MPTP-induced loss of tyrosine hydroxylase-positive (TH^+) mouse neurons in substantia nigra pars compacta (SNc). The potent efficacy of acalitide in mice suggested that it could be a drug candidate with prospective prospects in combating Parkinson's disease.

As a relatively young but diversely useful omics approach, metabolomics has found its expanding application in biomedicine (*e.g.*, biomarker identification)[36,37] and agriculture (*e.g.*, crop improvement)[38,39]. Adding to those objects, this work demonstrates the 'metabolomics prowess' in the first step of mining the first-in-class lead compound, acalitide, which may initialize the development of new peptide-based drug to treat PD, a clinically unsolved but globally prevailing disease. To our knowledge, acalitide is distinct from the counterparts found in fungi, plants, and bacteria[9,40−43], and represents the first RiPP macrotricyclized *via* two disulfide and an amide bonds from an undescribed precursor peptide (AcaA) (Figs. 1−3 and Table S1) whose N-terminal AA sequence is entirely different from the counterparts characterized earlier[7,9]. However, such advantages in the structure and biosynthesis of acalitide were accompanied by the poor productivity of its original fungal producer. The bottleneck was addressed by our establishment of an alternative access to acalitide by understanding and utilizing its biosynthetic logic (Figs. 3 and 4). As a matter of fact, it was such an acalitide supply renewal that facilitated its bio-evaluation in diverse models to identify consequently its neuroprotectivity in the *in vitro* and *in vivo* PD models (Fig. 5 and Table S5). Next, we were further challenged by how to properly deliver acalitide into brain. The frustration was overcome by our encapsulation of acalitide into a long-circulating liposome (Tf-Aca-LCL) (Figs. 6, 7A and B), which was evidenced to be safe (Supporting Information Fig. S16), and in particular, at least as efficacious as amantadine in the PD-suffering mice (Fig. 7C and D). Cumulatively, the work discovered and consolidated acalitide as an antiparkinsonian drug candidate through establishing or updating the paradigm about the discovery and druggability improvement of low-abundance natural products with unforeseeable chemical structures and biological functions.

3. Conclusions

The work presents the structure, biosynthesis, sample supply renewal, and promisingly antiparkinsonian efficacy of acalitide, which is the founding member of RiPPs macrotricyclized *via* an amide and two disulfide bonds from an undescribed precursor peptide (AcaA). The renewed acalitide supply achieved herein provided enough material for the 'compound-centric' bioassay in diverse models to lead to the identification of its *in vitro* and *in vivo* antiparkinsonian potency. The druggability of acalitide was further consolidated by ascertaining its safety and establishing its brain-targeted delivery system. In aggregation, the study has updated the RiPP category list, offered insights into the complexity of fungal RiPP biosynthesis, and provided a promising antiparkinsonian drug candidate valuable for managing

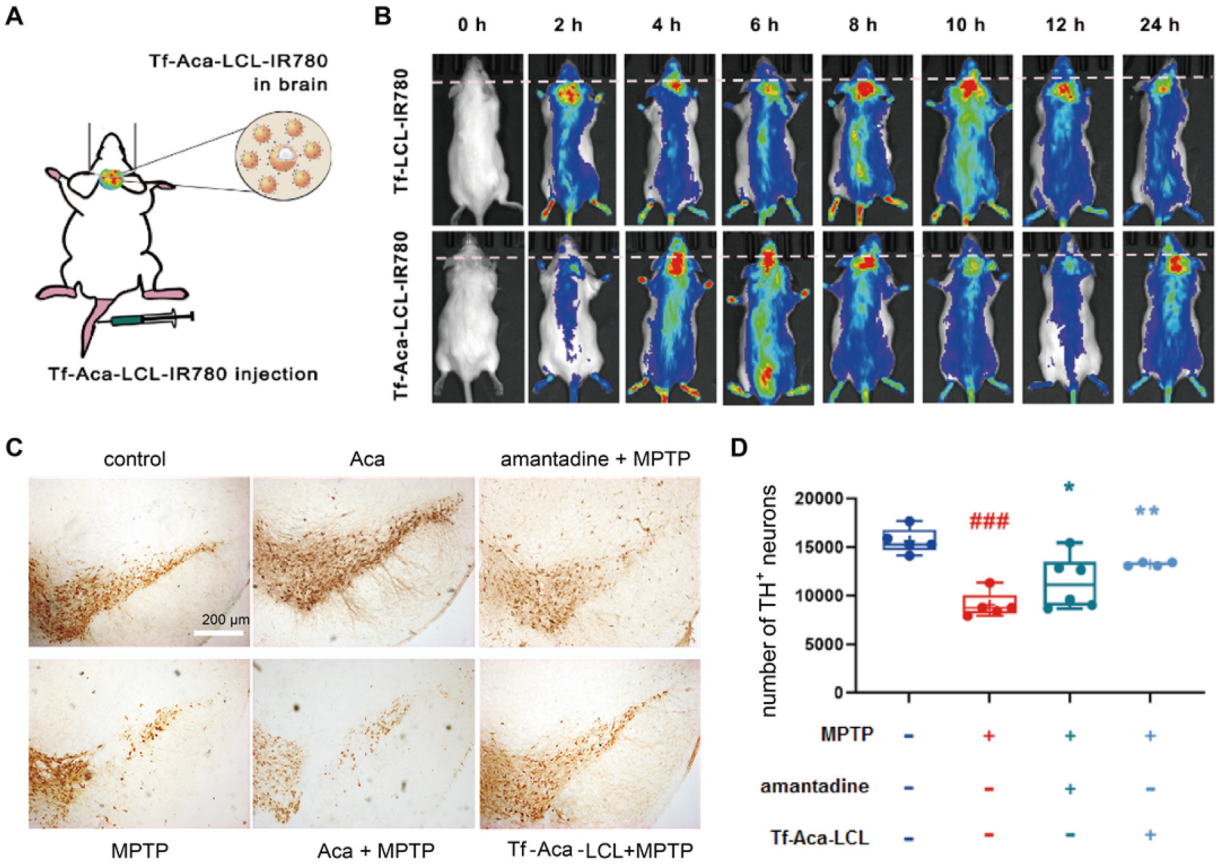

Figure 7 *In vivo* neuroprotectivity of acalitide (Aca). (A) Schematic diagram of a mouse PD model injected with Tf-Aca-LCL-IR780. (B) Tf-Aca-LCL-IR780 penetrated the blood−brain barrier (BBB) signifying that Tf-Aca-LCL is BBB-penetrable, too. Mice were injected with Tf-Aca-LCL-IR780 or Tf-LCL-IR780 *via* tail vein from 0 to 24 h and subjected to the *in vivo* fluorescence image acquisition from 0 to 24 h after injected. The Tf-LCL-IR780 and Tf-Aca-LCL-IR780 administered mice gave their bright fluorescence 4 and 2 h after the injection. (C−D) Acalitide counteracted the loss of midbrain dopamine neurons as evidenced from microphotographs (C) and stereo-logical counts (D) of tyrosine hydroxylase-positive (TH^+) neurons in substantia nigra pars compacta (SNc). MPTP: 30 mg/kg/day, Tf-Aca-LCL: 5 mg/kg/day, amantadine: 10 mg/kg/day. The data are the mean ± SEM. $^*P < 0.05$, $^{**}P < 0.01$, $^{***}P < 0.001$ *vs* MPTP group, $^{\#\#\#}P < 0.001$ *vs* control group are analyzed with One-way-ANOVA, $n = 4-6$ mice for each group. Aca, acalitide; MPP^+, 1-methyl-4-phenylpyridinium; MPTP, 1-methyl-4-phenyl-1,2,3,6-tetrahydropyridine; PD, Parkinson's disease; Tf-Aca-LCL and Tf-Aca-LCL-IR780, defined in the text.

Parkinson's disease and a paradigm (or strategy) applicable for characterizing less-abundant but high-valued compounds from Nature.

4. Experimental

4.1. General experimental procedures

Optical rotation was acquired on a Rudolph Research Analytical Autopol IV automatic polarimeter. CD spectra were measured on a JASCO-810 spectropolarimeter. All NMR spectra were recorded on a Bruker DRX-600 spectrometer using TMS as an internal standard. The ^1H and ^{13}C chemical shifts were described relative to the solvent pyridine-d_5 (δ_H 8.74, 7.58 and 7.22, and δ_C 150.3, 135.9 and 123.9). Reversed-phase HPLC purification was carried out on an ODS-2 Hypersil column (5 μmol/L, 250 mm × 10 mm). Column and thin-layer chromatographies were respectively accomplished on silica (200−300 mesh) and GF_{254} (10−20 μm) gels from Qingdao Marine Chemical Company, China. Reverse-phase column chromatography was performed over ODS-A gel (AA12S50; YMC Co., Ltd., Japan), and the gel filtration over Sephadex LH-20 (Pharmacia Biotech, Sweden), ultraviolet (UV) spectra were measured on a NanoDrop 2000c spectrometer (Thermo Technology).

4.2. Isolation and characterization of acalitide

A. album (Costantin) Seifert & Woudenb (=*Acalium* sp. H-JQSF mentioned elsewhere)[21−24] was isolated from *Armadillidium vulgare*, collected in Zhangjiakou city, Hebei Province, China. The living *A. vulgare* was immersed in 75% ethyl alcohol for 15 min, and the residual ethyl alcohol was drained off with filter paper before grinded with 1 mL sterile water, followed by a 10-fold dilution using the same water. The obtained liquor (0.2 mL) was evenly coated on plates containing modified Czapek's medium (sucrose 3.0 g, Na_2NO_3 3.0 g, $MgSO_4 \cdot 7H_2O$ 0.5 g, $FeSO_4 \cdot 7H_2O$ 0.001 g, KH_2PO_4 1.0 g, KCl 0.5 g, yeast extract 1.0 g, kanamycin 150 mg, ampicillin sodium 150 mg, agar powder 20.0 g and H_2O up to a total volume of 1 L), modified potato dextrose agar (mPDA, potato 20.0 g, glucose 2.0 g, kanamycin 150 mg, ampicillin sodium 150 mg, agar powder 20.0 g and H_2O up to a total volume of 1 L), modified water agar (agar powder 20.0 g, kanamycin 150 mg, ampicillin sodium 150 mg and H_2O up to a total volume of 1 L). A month later, the same

fungal colonies on diverse plates were selected and domesticated on PDA (20.0 g glucose, 200 g potato, 20.0 g agar, and H_2O up to a total volume of 1 L). The taxonomic identification of the fungus was done on its ITS sequence which is comparable to that of *Acalium* genus available in the China General Microbiological Culture Collection Center.

Ascertaining the peptide (acalitide) in the mother liquor left during previous investigation of the *A. album* metabolites[21−24], the fungus was re-cultivated on PDA for 6 days at 28 °C on a larger scale. Briefly, the mycelia were sliced into squares ($0.5 \times 0.5 \times 0.5$ cm^3) and incubated in 500 mL Erlenmeyer flasks containing 150 mL with liquid medium (yeast extract 10 g, polypeptone 10 g, casaminoacid 10 g, sucrose 10 g and H_2O up to a total volume of 1 L, pH 6.8), followed by shaking at 120 rpm for 4 days at 30 °C. The fungal culture was incubated in 1 L Erlenmeyer flasks on a rice solid medium (rice 80 g and distilled water 120 mL for each of the 50 flasks), followed by a static incubation for 30 days at 30 °C. The culture broth was then extracted with EtOAc (*v*/*v*, 1:1). Evaporation of solvent from the extract under reduced pressure yielded 28 g residue, which was separated by column chromatography (CC) over silica gel eluted with polarity-growing EtOAc/MeOH mixtures (*v*/*v*, 100:0 → 0:100) to give ten fractions (Fr.1−Fr.10). Separation of Fr.10 (68 mg) by CC over ODS-A gave eight fractions (Fr.10.1−Fr.10.8). Re-purification of Fr.10.4 (32 mg) by RP-HPLC with MeOH/H_2O (87:13), flow rate 2 mL/min, retention time 18 min, afforded acalitide (6.0 mg), yield of 0.021%.

4.3. Heterologous expression of acalitide

For the acalitide expression in *A. oryzae* NSAR1 (shortened as 'AO'), the full-length *acaA* and *acaB* genes were amplified from the *A. album* genome using primers listed in Supporting Information Table S3, with Phanta Max Super-Fidelity DNA Polymerase. Based on homologous recombination, the resultant fragments *acaA* and *acaB* (NCBI accession number: OP150447) were respectively introduced into the KpnI-linearized vectors pTAex3 and pUSA using Clone Express Ultra One Step Cloning Kit. The expression plasmids were transformed into AO by the polyethyleneglycol (PEG)-mediated transformation, and the corresponding empty vectors were also transformed into AO as a negative control. Likewise, the *acaAB* genes were introduced into the XbaI-linearized vector pAdeA using Clone Express Ultra One Step Cloning Kit, and transformed into AO-*acaAB* transformant to form the double-copy (AO-2 × *acaAB*) transformant. The positive transformant was verified by PCR and fermented in 1 L erlenmeyer flasks on modified martin broth medium (MMB; yeast extract 10.0 g/L, peptone 10.0 g/L, maltose 20.0 g/L, KH_2PO_4 1.0 g/L, $MgSO_4 \cdot 7H_2O$ 0.5 g/L), incubation for 3 days at 30 °C and 220 rpm, 400 mL per bottle, total of 50 bottles. The culture broth was then extracted with EtOAc (*v*/*v*, 1:1). Evaporation of solvent from the extract under reduced pressure yielded 18 g residue. Using the above-mentioned method, afforded acalitide (114.0 mg), yield of 0.63%.

4.4. Site-directed mutagenesis of AcaA

Site-directed mutains AO-$acaA^{G58A}B$ and AO-$acaA^{G28A}B$ were using primers listed in Supporting Information Table S3, with Phanta Max Super-Fidelity DNA Polymerase. The site-directed mutains expression plasmids were transformed into AO-acaA transformant to form the AO-$acaA^{G58A}B$ and AO-$acaA^{G28A}B$ mutains. The mutains were verified and fermented using the same method as described above.

4.5. Cell viability assay

According to the manufacturer's instructions, the cell viability was measured by Cell Counting Kit-8 (CCK-8, Bimake, B34304). Briefly, 5×10^3 SH-SY5Y cells per well were seeded in a 96-well plate and treated, after a 1-h exposure to acalitide, with MPP^+ (Sigma−Aldrich, D048) for 24 h. CCK-8 reagent (10 μL) was added to each well, and after standing for 2.5 h, the absorbance was measured at 450 nm using Varioskan Flash (Thermo Fisher Scientific, Waltham, Massachusetts, USA), and analyzed by Thermo Scientific™ Skanlt™ software (Thermo Fisher Scientific, Waltham, MA, USA).

4.6. Cell immunofluorescence experiment

After treated with MPP^+ and acalitide, mouse primary neurons were rinsed thrice with 0.01 mol/L PBS and fixed in 4% paraformaldehyde, followed by blockage with PBS containing 5% bovine serum albumin (BSA) for 2 h at room temperature. After rinsed by PBS again, primary antibody (MAP2, Proteintech, #17490-1-AP, 1:300) was added. The ensuing incubation overnight at 4 °C was followed by addition of the corresponding secondary antibody (Alexa Fluor 555 goat anti-mouse, 1:1000, #A21422, Invitrogen; Alexa Fluor 488 Goat anti-Rabbit, #A11008, 1:1000, Invitrogen). After incubated for 2 h at room temperature, rinsed with PBS, and stained with Hoechst33342 (Sigma, #B2261), the cells were observed under a stereomicroscope (Olympus, Tokyo, Japan).

4.7. Annexin V-FITC/propidium (AV/PI) flow cytometry

Apoptosis of SH-SY5Y cells was detected using Annexin V-FITC/propidium iodide (AV/PI) fluorescent dye (Vazyme, A211-01). After 10-min treatment, cells were digested by 0.25% Trypsin solution without ethylenediaminetetraacetic acid (EDTA) for 1 min and collected at 4 °C by centrifugation at 1000 rpm. After washed with sterile phosphate buffer saline (PBS), the cells were resuspended in 50 μL binding buffer, stained with 5 μL AV and 5 μL PI dye at room temperature for 10 min, and added 400 μL binding buffer in cell suspension for the flow cytometry analysis. The data were analyzed with the FCS Express™ software (Guava Easy Cyte8, Millipore, USA).

4.8. Neuroprotectivity assay of Aca in nematode

The nematode used in this study was *C. elegans* BZ555 [dat-1pGFP] (GFP stands for green fluorescent protein), which was donated by Jun Guo Laboratory, Nanjing University of Chinese Medicine. The nematode strain BZ555 strain has eight dopamine neurons, of which six in the head and two posteriors. The dopamine neurons become visualizable because of their expression of GFP under the promotion of dat-1, a dopamine neuron-specific promoter. Thus the GFP fluorescence decreases when dopamine neurons are injured or lost.

The BZ555 strain was propagated at 21 °C on solid nematode growth media (NGM) seeded with the *E. coli* OP50, on which it feeds. After incubated for 3 days after hatching, the nematodes were treated with MPP^+ (2 mmol/L, Sigma, D048) and Aca (2 μmol/L) for 48 h, and placed on glass slides with 10 μL

levamisole, and visualized with a fluorescence microscope fitted with a camera.

4.9. *C. elegans lifespan test*

After synchronization, nematodes were placed on NGM plates with the *E. coli* OP50 and picked to new plates, and scored every 2 days until they died off.

4.10. *Swimming-induced paralysis (SWIP) assay*

Under the stereoscope, 8−10 late-L4 stage *C. elegans* were picked with eyelash or platinum pickers. The nematodes were moved off for swimming by submerging the picker into PBS. The nematodes exhibiting swimming induced paralysis were counted at every 2 min in a 10-min duration followed by the percentage calculation.

4.11. *Size-controlled preparation of Tf-Aca-LCL, Tf-LCL and Tf-Aca-LCL-IR780*

Synthesis of Tf-Aca-LCL. In a 2-liter round-bottom distillation flask, 120 mg acalitide was evenly mixed with 40 mL dichloromethane, 60 mL methanol, 200 mg cholesterol, 1200 mg egg lecithin, 180 mg 1,2-distearoyl-*sn*-glycero-3-phosphoethanolamine-*N*-[methoxy(polyethylene glycol)-2000] (DSPE-PEG2000) and its glycolate (DSPE-PEG2000-COOH, 20 mg). Evaporation of dichloromethane and methanol at 35 °C under reduced pressure gave a thin film, which was dissolved in 100 mL PBS buffer and sonicated in an ultrasonic mill for 20 min to afford the primary emulsion, being homogenized on a high pressure homogenizer to obtain Aca-LCL. Subsequently Aca-LCL (85 mL) was stirred at room temperature for 10 min with 29 mg *N*-ethyl-*N*′-(3-dimethylaminopropyl) carbodiimide (EDC), 48.2 mg *N*-hydroxysuccinimide (NHS), and 20 mg DSPE-PEG2000-COOH, followed by addition of 10 mg DSPE-PEG2000-COOH and 70 mg transferrin. After incubating at 37 °C for 3 h, the reaction mixture was centrifuged using a 100 kD ultrafiltration tube to afford Tf-Aca-LCL as a concentrate free of low-molecular-weight impurities.

4.12. *Synthesis of Tf-LCL and Tf-Aca-LCL-IR780*

Using the size-controlled synthetic protocol described above, we were able to prepare the drug-free liposome vector (Tf-LCL) and the fluorescent mimic (Tf-Aca-LCL-IR780) by the deprival of acalitide and the addition of a 15:1 mixture of acalitide and IR780 iodide in the first step toward synthesizing Tf-Aca-LCL, respectively.

4.13. *Experimental procedures of acalitide neuroprotectivity in vivo*

All animal care and procedures were performed according to the national and international guidelines and were approved by the Animal Resource Centre, Nanjing Medical University. All authors complied with the relevant ethical regulations for animal testing and research. Mice were housed in groups (2−5 siblings) at 22−24 °C with a 12 h light−dark cycle, and freely accessible to a regular chow diet and water. Adult or neonatal mice were purchased from the Model Animal Research Center of Nanjing Medical University.

Three-month-old C57BL/6 mice were used to generate a subacute PD model by injecting hypodermically (i.h.) 30 mg/kg MPTP (1-methyl-4-phenyl-1,2,3,6-tetrahydropyridine, dissolved in saline) (Selleck, S473204), once a day for consecutive 5 days followed by being kept alone for 3 days. One day ahead of the first-time MPTP injection, mice in the Tf-Aca-LCL and amantadine-treated groups were given, once a day for 9 consecutive days, *via* tail-vein injection of Tf-Aca-LCL (5 mg/kg acalitide) and 10 mg/kg amantadine, respectively. Three days after the last injection, the brains of test mice were fixed with 4% paraformaldehyde in 0.1 mol/L phosphate buffer (pH 7.4) to make cryo-sections at a thickness of 30 mm. The midbrain cryo-sections were prepared and processed for immunocytochemistry.

To study the BBB transportability of Tf-Aca-LCL-IR780, eight-week-old ICR mice were injected with Tf-Aca-LCL-IR780 or vehicle at 0, 2, 4, 6, 8, 10, 12 and 24 h before acquiring fluorescence images by IVIS® Spectrum (PerkinElmer, Massachusetts, USA). The corresponding fluorescence intensities were analyzed by Living Image Software.

4.14. *Immunohistochemistry (IHC) analysis*

Mice treated differently were anesthetized with pentobarbital sodium (Sigma−Aldrich, P-010) and perfused with PBS till blood disappeared. Mouse brains were harvested and fixed in 4% paraformaldehyde, followed by successive dehydration in 20% sucrose-PBS and 30% sucrose-PBS. The brains were cut into frozen slices (30 μmol/L). After rinsed with PBS, the sections were treated with 3% H_2O_2 for 15 min to quench endogenous peroxidase activity, permeabilized, and blocked with 0.3% Triton X-100 in PBS containing 5% BSA for 1.5 h at room temperature. Then, the slices were incubated with primary tyrosine hydroxylase (TH) antibody (Sigma−Aldrich, T1299) at 4 °C overnight, and the results were visualized by the 3,3′-diaminobenzidine (DAB) reaction.

Acknowledgments

The work was co-financed by the NSFC (81991524, 81991523, and 22193071, China) and MOST grants (STI2030-Major Project-2022ZD0211804, China). We thank Profs. Jinhui Wu at Nanjing Univ. for his technical advice for the liposome preparation and K. Gomi at Tohoku Univ. for providing *Aspergillus oryzae* NSAR1 and expression vectors pTAex3, pUSA, and pAdeA.

Author contributions

Zhiwu Tong, Xiahong Xie, Gang Hu and Renxiang Tan designed experiments and wrote the manuscript with feedback from all authors; Zhiwu Tong conducted fermentation, characterization, synthetic biology and chemical preparation with help from Huiming Ge and Ruihua Jiao; Zhiwu Tong and Xiahong Xie performed bio-evaluation and elucidated mode of action; Tingting Wang, Xincun Wang and Wenying Zhuang isolated and identified the fungus.

Conflicts of interest

The authors declare no conflict of interest.

Appendix A. Supporting information

Supporting data to this article can be found online at https://doi.org/10.1016/j.apsb.2023.09.006.

References

1. Sharma K, Sharma KK, Sharma A, Jain R. Peptide-based drug discovery: current status and recent advances. *Drug Discov Today* 2023; **28**:103464.
2. Zhang H, Chen S. Cyclic peptide drugs approved in the last two decades (2001-2021). *RSC Chem Biol* 2021;**3**:18−31.
3. Graham WV, Bonito-Oliva A, Sakmar TP. Update on Alzheimer's disease therapy and prevention strategies. *Annu Rev Med* 2017;**68**: 413−30.
4. Grover T, Mishra R, Bushra Gulati P, Mohanty A. An insight into biological activities of native cyclotides for potential applications in agriculture and pharmaceutics. *Peptides* 2021;**135**:170430.
5. Arnison PG, Bibb MJ, Bierbaum G, Bowers AA, Bugni TS, Bulaj G, et al. Ribosomally synthesized and post-translationally modified peptide natural products: overview and recommendations for a universal nomenclature. *Nat Prod Rep* 2013;**30**:108−60.
6. Luo SW, Dong SH. Recent advances in the discovery and biosynthetic study of eukaryotic RiPP natural products. *Molecules* 2019;**24**: 1541−56.
7. Montalbán-López M, Scott TA, Ramesh S, Rahman IR, van Heel AJ, Viel JH, et al. New developments in RiPP discovery, enzymology and engineering. *Nat Prod Rep* 2021;**38**:130−239.
8. Hallen HE, Luo H, Scott-Craig JS, Walton JD. Gene family encoding the major toxins of lethal amanita mushrooms. *Proc Natl Acad Sci U S A* 2007;**104**:19097−101.
9. Kessler SC, Chooi YH. Out for a RiPP: challenges and advances in genome mining of ribosomal peptides from fungi. *Nat Prod Rep* 2022; **39**:222−30.
10. Kessler SC, Zhang XH, McDonald MC, Gilchrist CLM, Lin Z, Rightmyer A, et al. Victorin, the host-selective cyclic peptide toxin from the oat pathogen cochliobolus victoriae, is ribosomally encoded. *Proc Natl Acad Sci U S A* 2020;**117**:24243−50.
11. Ye Y, Ozaki T, Umemura M, Liu CW, Minami A, Oikawa H. Heterologous production of asperipin-2a: proposal for sequential oxidative macrocyclization by a fungi-specific DUF3328 oxidase. *Org Biomol Chem* 2018;**17**:39−43.
12. Nagano N, Umemura M, Izumikawa M, Kawano J, Ishii T, Kikuchi M, et al. Class of cyclic ribosomal peptide synthetic genes in filamentous fungi. *Fungal Genet Biol* 2016;**86**:58−70.
13. Ye Y, Minami A, Igarashi Y, Izumikawa M, Umemura M, Nagano N, et al. Unveiling the biosynthetic pathway of the ribosomally synthesized and post-translationally modified peptide ustiloxin B in filamentous fungi. *Angew Chem Int Ed* 2016;**55**:8072−5.
14. Sogahata K, Ozaki T, Igarashi Y, Naganuma Y, Liu CW, Minami A, et al. Biosynthetic studies of phomopsins unveil posttranslational installation of dehydroamino acids by UstYa family proteins. *Angew Chem Int Ed* 2021;**60**:25729−34.
15. Velden NS, Kälin N, Helf MJ, Piel J, Freeman MF, Künzler M. Autocatalytic backbone *N*-methylation in a family of ribosomal peptide natural products. *Nat Chem Biol* 2017;**13**:833−5.
16. Ramm S, Krawczyk B, Mühlenweg A, Poch A, Mösker E, Süssmuth RD. A self-sacrificing *N*-methyltransferase is the precursor of the fungal natural product omphalotin. *Angew Chem Int Ed* 2017; **56**:9994−7.
17. Sterner O, Etzel W, Mayer A, Anke H. Omphalotin, a new cyclic peptide with potent nematicidal activity from *omphalotus olearius* II. isolation and structure determination. *Nat Prod Lett* 1997;**10**:33−8.
18. Liermann JC, Opatz T, Kolshorn H, Antelo L, Hof C, Anke H, et al. Five oxidatively modified nematicidal cyclopeptides from *omphalotus olearius*. *Eur J Org Chem* 2009;**2009**:1256−62.
19. Gauhe A, Wieland T, Über Die Inhaltsstoffe Des Grünen Knollenblätterpilzes LI. Die cycloamanide, monocyclische peptide; isolierung und strukturaufklärung eines cyclischen heptapeptids (CyA B) und zweier cyclischer oktapeptide (CyA C und CyA D). *Liebigs Ann Chem* 1977;**1977**:859−68.
20. Pulman JA, Childs KL, Sgambelluri RM, Walton JD. Expansion and diversification of the MSDIN family of cyclic peptide genes in the poisonous agarics *amanita phalloides* and *A. bisporigera*. *BMC Genom* 2016;**17**:1038−52.
21. Tong ZW, Wang TT, Yang P, Sun JL, Zhang CP, Khan S, et al. Acatulides A−G, neuroprotective macrolides from *Acaulium album* H-JQSF. *Chin Chem Lett* 2023:108488.
22. Tong ZW, Xie XH, Wang TT, Lu M, Jiao RH, Ge HM, et al. Acautalides A−C, neuroprotective Diels−Alder adducts from solid-state cultivated *Acaulium* sp. H-JQSF. *Org Lett* 2021;**23**:5587−91.
23. Wang TT, Wei YJ, Ge HM, Jiao RH, Tan RX. Acaulins A and B, trimeric macrodiolides from *Acaulium* sp. H-JQSF. *Org Lett* 2018;**20**: 2490−3.
24. Wang TT, Wei YJ, Ge HM, Jiao RH, Tan RX. Acaulide, an osteogenic macrodiolide from *Acaulium* sp. H-JQSF, an isopod-associated fungus. *Org Lett* 2018;**20**:1007−10.
25. Daly NL, Rosengren KJ, Craik DJ. Discovery, structure and biological activities of cyclotides. *Adv Drug Deliv Rev* 2009;**61**:918−30.
26. Weissman JS, Kim PS. Efficient catalysis of disulphide bond rearrangements by protein disulphide isomerase. *Nature* 1993;**365**:185−8.
27. Gruber CW, Cemazar M, Heras B, Martin JL, Craik DJ. Protein disulfide isomerase: the structure of oxidative folding. *Trends Biochem Sci* 2006;**31**:455−64.
28. Chalorak P, Jattujan P, Nobsathian S, Poomtong T, Sobhon P, Meemon K. Holothuria scabra extracts exhibit anti-Parkinson potential in *C. elegans*: a model for anti-Parkinson testing. *Nutr Neurosci* 2018; **21**:427−38.
29. Thomas B, Coelln R, Mandir AS, Trinkaus DB, Farah MH, Lim KL, et al. MPTP and DSP-4 susceptibility of substantia nigra and locus coeruleus catecholaminergic neurons in mice is independent of parkin activity. *Neurobiol Dis* 2007;**26**:312−22.
30. Xiong S, Li ZJ, Liu Y, Wang Q, Luo JS, Chen XJ, et al. Brain-targeted delivery shuttled by black phosphorus nanostructure to treat Parkinson's disease. *Biomaterials* 2020;**260**:120339.
31. Hu J, Wang JJ, Wang G, Yao ZJ, Dang XQ. Pharmacokinetics and antitumor efficacy of DSPE-PEG2000 polymeric liposomes loaded with quercetin and temozolomide: analysis of their effectiveness in enhancing the chemosensitization of drug-resistant glioma cells. *Int J Mol Med* 2016;**37**:690−702.
32. Hu WD, Mao A, Wong P, Larsen A, Yazaki PJ, Wong JYC, et al. Characterization of 1,2-distearoyl-*sn*-glycero-3-phosphoethanolamine-*N*-[methoxy(polyethylene glycerol)-2000] and its complex with doxorubicin using nuclear magnetic resonance spectroscopy and molecular dynamics. *Bioconjugate Chem* 2017;**28**:1777−90.
33. Seo JW, Ang JC, Mahakian LM, Tam S, Fite B, Ingham ES, et al. Self-assembled 20-nm (64)Cu-micelles enhance accumulation in rat glioblastoma. *J Contr Release* 2015;**220**:51−60.
34. Salas CG, Rodríguez BF, Pardo JAP, Rojas RR, Obeso I, Fernández FH, et al. Blood−brain barrier opening with focused ultrasound in Parkinson's disease dementia. *Nat Commun* 2021;**12**:779−85.
35. Milanese C, Gabriels S, Barnhoorn S, Cerri S, Ulusoy A, Gornati SV, et al. Gender biased neuroprotective effect of transferrin receptor 2 deletion in multiple models of Parkinson's disease. *Cell Death Differ* 2021;**28**:1720−32.
36. Khomiak A, Brunner M, Kordes M, Lindblad S, Miksch RC, Öhlund D, et al. Recent discoveries of diagnostic, prognostic and predictive biomarkers for pancreatic cancer. *Cancers* 2020;**12**:3234.
37. Caspani G, Sebők V, Sultana N, Swann JR, Bailey A. Metabolic phenotyping of opioid and psychostimulant addiction: a novel approach for biomarker discovery and biochemical understanding of the disorder. *Br J Pharmacol* 2022;**179**:1578−606.
38. Darkwa K, Olasanmi B, Asiedu R, Asfaw A. Review of empirical and emerging breeding methods and tools for yam (*Dioscorea* spp.) improvement: status and prospects. *Plant Breed* 2020;**139**:474−97.
39. Scossa F, Alseekh S, Fernie AR. Integrating multi-omics data for crop improvement. *J Plant Physiol* 2021;**257**:153352.

40. Zhong GN, Wang ZJ, Yan F, Zhang YM, Huo LJ. Recent advances in discovery, bioengineering, and bioactivity-evaluation of ribosomally synthesized and post-translationally modified peptides. *ACS Bio Med Chem Au* 2022;**3**:1−31.
41. Imai Y, Meyer KJ, Iinishi A, Favre-Godal Q, Green R, Manuse S, et al. A new antibiotic selectively kills gram-negative pathogens. *Nature* 2019;**576**:459−64.
42. Saad H, Aziz S, Gehringer M, Kramer M, Straetener J, Berscheid A, et al. Nocathioamides, uncovered by a tunable metabologenomic approach, define a novel class of chimeric lanthipeptides. *Angew Chem Int Ed* 2021;**60**:16472−9.
43. Elashal HE, Cohen RD, Zong CH, Link AJ, Raj M. Cyclic and lasso peptides: sequence determination, topology analysis, and rotaxane formation. *Angew Chem Int Ed* 2018;**57**:6150−4.